Testing the Mid-Holocene Relative Sea-Level Highstand Hypothesis in North Wales, United Kingdom

Greg T. Rushby[1], Geoff T. Richards[2], W. Roland Gehrels[2], William P. Anderson, Jr[3], Mark D. Bateman[1], William H. Blake[4]

As accepted to The Holocene (10/5/19) HOL-19-0036.R1.

1. Geography Department, University of Sheffield, Winter St. Sheffield S10 2TN, UK

2. Department of Environment and Geography, University of York, Heslington, York, YO10 5NG, UK

3. Department of Geological and Environmental Sciences, Appalachian State University, 572 Rivers Street, Boone, NC 28608, USA

4. School of Geography, Earth and Environmental Sciences, Plymouth University, Plymouth, Devon, PL4 8AA, UK

Email: gtrushby1@sheffield.ac.uk (corresponding), geoffrey.t.richards@durham.ac.uk, roland.gehrels@york.ac.uk, andersonwp@appstate.edu, m.d.bateman@sheffield.ac.uk, william.blake@plymouth.ac.uk

Abstract

Accurate Holocene relative sea-level curves are vital for modelling future sea-level changes, particularly in regions where relative sea-level changes are dominated by isostatically induced vertical land movements. In north Wales, various glacio-isostatic adjustment (GIA) models predict a Mid-Holocene relative sea-level highstand between 4-6 ka which is unsubstantiated by any geological sea-level data but affects the ability of geophysical models to model accurately past and future sea level. Here we use a newly developed foraminifera-based sea-level transfer function to produce a 3,300 year long Late Holocene relative sea-level reconstruction from a salt marsh in the Malltraeth estuary on the south Anglesey coast in north Wales. This is the longest continuous Late Holocene relative sea-level reconstruction in north-west Europe. We combine this record with two new Late Holocene sea-level index points (SLIPs) obtained from a freshwater marsh at Rhoscolyn, Anglesey, and with previously published regional SLIPs, to produce a relative sea-level record for north Wales that spans from ca. 13,000 BP to the present. This record leaves no room for a Mid-Holocene relative sea-level highstand in the region. We conclude that GIA models that include a Mid-Holocene sea-level highstand for north Wales need revision before they are used in the modelling of past and future relative sea-level changes around the British Isles.

Keywords

Glacio-isostatic adjustment (GIA), Irish Sea, Salt Marsh, Foraminifera, Groundwater,

1. Introduction

Due to the spatial variability in the processes that drive relative sea-level (RSL) change at the coast, high quality regional Holocene relative sea-level data are required to enable a thorough understanding of the processes driving past and future coastal change. This is especially true for the British Isles where the unique interactions between the British and Irish Ice Sheet (BIIS) and the Fennoscandian Ice Sheet result in diverse isostatically driven Holocene sea-level histories (Shennan et al. 2018). This, along with the abundance of sedimentary archives of sea-level data around the UK coast, has led to the construction of a consolidated UK and Ireland sea-level index-point (SLIP) database (Shennan et al. 2006; Shennan et al. 2018) that has been central to the development and validation of a series of quantitative glacial isostatic adjustment (GIA) models of the UK and NW Europe (Bradley et al. 2011; Milne et al. 2006; Shennan et al. 2006). These GIA models are vital tools for simulating the response of the solid Earth to mass transfer between the oceans and the cryosphere; constraining ice-sheet thickness, extent and dynamics; and quantifying global meltwater flux and the viscosity structure of the Earth's mantle (Bradley et al. 2011; Milne et al. 2006; Uehara et al. 2006). Due to their ability to predict vertical land movements along the coast, GIA models are also key to predicting future relative sea-level changes around the British Isles (Gehrels, 2010; Shennan et al. 2011).

In areas where the temporal coverage of empirical RSL data is sparse, GIA models remain poorly validated and there may be a resultant mismatch between GIA sea-level predictions and empirical (geological) RSL data. North Wales has been identified as poor agreement between some GIA models and empirical SLIPs (Roberts et al. 2011; Shennan et al. 2006; Brooks et al. 2008). This mismatch has led to a debate on the southern-most limit of a ~1-2 m Mid-Holocene sea-level highstand (Peltier, 2002; Shennan et al. 2006), the existence of which is supported by sea-level index points further north on the coast of north-west England (Lloyd et al. 2013). Some models, notably that of Lambeck (1996), suggest that Mid-Holocene RSL was not higher than present in north Wales, whilst others predict a Mid-Holocene highstand, in particular the ICE-4G and ICE-5G iterations by Peltier (1994) and Peltier (2004), which both predict RSL maxima of 1.33 m at 4 ka and 0.93 m at 4 ka, respectively. More recent models such as BRADLEY2011 (Bradley et al. 2011) and its more recent iteration BRADLEY2017 (Shennan et al. 2018) also predict a Mid-Holocene highstand in north Wales, albeit of smaller magnitude. Constraining the southern-most limit of Mid-Holocene emergence is of importance for the validation and future refinement of GIA models for investigating both RSL, ice-loading histories and earth rheology (Bradley et al. 2016).

The Holocene RSL history of north Wales is one of the least well understood in the UK with no continuous record and most SLIPs for the region only being of Early to Mid-Holocene in age, and little data constraining relative sea level in the Late Holocene (Shennan et al. 2018). Until the study by Roberts et al. (2011), the empirical RSL data for north Wales comprised of only 12 SLIPs and one limiting point (Bedlington, 1994; Heyworth and Kidson, 1982; Prince, 1988; Shennan et al. 2006). Roberts et al. (2011) expanded upon this greatly with the addition of ten new SLIPs and nine limiting dates derived from estuarine sequences in the NE Menai Strait. Despite this step forward in understanding of RSL in north Wales, any high-resolution appraisal of Late Holocene relative sea-level changes remains limited, as the most recent SLIP in the Roberts et al. (2011) dataset is dated to 4.25-4.83 ka BP.

The goal of this study is to better constrain the southern-most limit of Mid-Holocene emergence by expanding upon the north Wales sea-level dataset with data from the Late Holocene (4 ka BP to present) to test the Mid-Holocene highstand hypothesis in north Wales. The objectives of this study are to: (1) produce the first high-resolution Late Holocene relative sea-level reconstruction for north Wales from a 3,300-year long salt-marsh sedimentary sequence believed to be the longest continuous salt-marsh sequence in the UK; (2) combine this reconstruction with additional basal SLIPs derived from a nearby tidally influenced backbarrier freshwater marsh, using a novel groundwater modelling approach; (3) combine these data with regional SLIPs derived from previous studies (Roberts et al. 2011; Shennan et al. 2006; Shennan et al. 2018) and produce complete Holocene relative sea-level history for north Wales; and (4) compare the relative sea-level history of North Wales with various GIA model predictions to assess their ability to accurately simulate north Wales Holocene relative sea-level changes.

2. Study area

2.1. North Wales

The coastlines of north Wales and the Isle of Anglesey have great variety in their geomorphology, from sheer cliffs and high energy beaches to extensive dunes and sandy estuaries. Most of the latter are constrained to the relatively sheltered areas surrounding the Menai Strait. The southern coast of Anglesey is predominantly subject to onshore south-westerly winds and waves. Tides are semi-diurnal with a mean tidal range of 3.72m recorded at Holyhead tide gauge.

Contemporary vertical land motion along the north Wales coastline based on interpolated Continuous Global Positing Satellite (CGPS) data carries large uncertainties and is estimated to be between -0.4 and 0.4 $mmyr^{-1}$ (Bradley et al. 2009). The vertical land motion rate becomes increasingly negative moving south due to the combined effects of the response to the BIIS and Fennoscandian ice sheets (Bradley et al. 2009; Simon et al. 2018).

2.2. Malltraeth salt marsh

Malltraeth salt marsh (53°10′21″N, 4°23′0″W) is situated on the eastern side of the Malltraeth estuary on the south Anglesey coast (Fig. 1.). The estuary overlies beds of Namurian (Middle Carboniferous) grits and sandstones and is flanked at its mouth by igneous rocks of the Gwna group (Horak and Evans, 2011). The estuary is one of the few low-energy depositional coastal environments in north Wales that harbour substantial salt marshes, owing to the shelter provided by the western Newborough dunes extending across the estuary's mouth. The marsh forms part of the Newborough Warren National Nature Reserve maintained by Natural Resources Wales. This reserve is mostly comprised of open sand dunes extending along the Abermenai Point spit in the east, and afforested dunes to the west. Trees were planted atop the dunes between 1947 and 1965 originally as an effort to stabilize the dunes and protect the village of Newborough from wind-blown sand (Rhind et al. 2001).

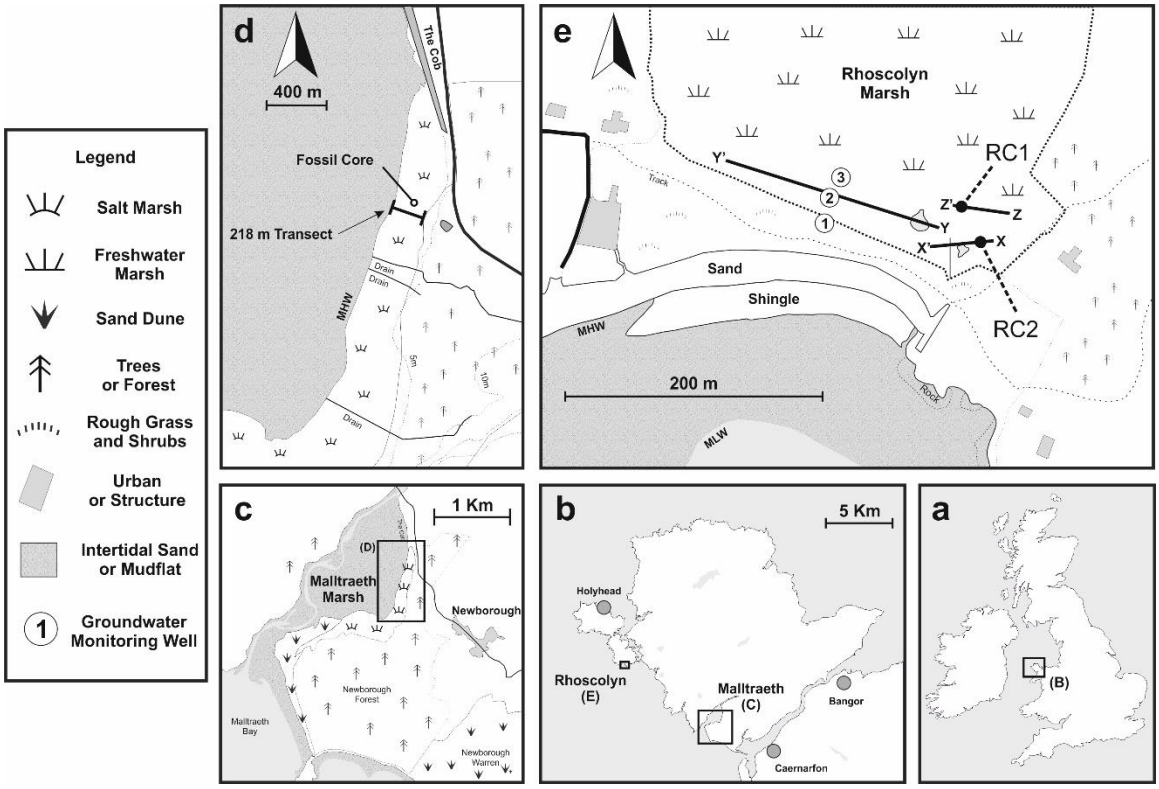

Figure 1. Location map of study sites and sampling strategies. a. United Kingdom, b. Isle of Anglesey, c. Malltraeth estuary and surrounding area, d. North portion of Malltraeth salt marsh and sampling locations, e. Rhoscolyn freshwater marsh and sampling locations.

The contemporary salt marsh is 0.9 km^2 in area. The northernmost extent of the marsh is bound by a sea wall known as the "Cob", by woodland to the east and the afforested dunes to the south. The marsh was once part of a much larger (1600 ha) marsh system extending north into a much larger estuary (Clout, 2007). This estuary and area of marsh was reclaimed in the early 1800s with the construction of the Cob (Packham and Liddle, 1970). Packham and Liddle (1970) suggest that following straightening of the Cefni channel in 1945 sedimentation in estuary was altered and resulted in the rapid lateral expansion of the southern part of the Malltraeth marsh. The southern area of the marsh has also contained a number of artificial drainage ditches in the past and, since the 1940s, a decoy pond. Given the potential complexities of rapid sedimentation and human influences, the southern portion of the marsh was avoided. Instead the area of the marsh shown in Fig. 1 was chosen to collect cores and to construct sea-level transfer functions from surface foraminiferal samples. Human influence was notably minimal in this area of the marsh and there is little evidence in the stratigraphy of former tidal creeks. The gradient from upper salt-marsh vegetation to the unvegetated tidal flat occurs over ~220 m and a ~1.5 m change in elevation.

2.3 Rhoscolyn freshwater marsh

The second site used in this study, Rhoscolyn marsh (53°14′44″N, 4°35′18″W) on Holy Island in western Anglesey, is a back-barrier freshwater marsh fronted by Borth Wen beach. The site extends approximately 0.55 km inland and covers an area of around 300 km^2. The vegetation is dominated by *Phragmites australis* and drainage is via a single culvert, which exits below the sand barrier through a tidal sluice. A small pond is present in the south east of the marsh. The fronting beach is predominantly sandy, leading to a rocky shoreline to the south. The Rhoscolyn back-barrier system overlies Late Precambrian rocks comprising the South Stack and New Harbour Groups. These consist of the interbedded psammites and pelites of the South Stack Group and the pelites of the New Harbour Group (Collins and Buchan, 2004; Hassani et al. 2004; Lisle, 1988). The freshwater peat is mostly underlain by glacial till.

3. Methodology

3.1. Salt-marsh sea-level reconstruction

Owing to the varying frequency of tidal inundation from high to low marsh, salt marshes typically exhibit strong zonation in their flora and fauna. Many studies have shown that in salt marshes tidal inundation represents the primary control on the distribution of microfauna, such as foraminifera and diatoms, that can therefore serve as proxies for sea-level change (Edwards et al. 2004; Patterson et al. 2004; Roe et al. 2009; Scott and Medioli, 1978) and act as “Late Holocene tide gauges” (Barlow et al. 2014; Barlow et al. 2013; Edwards and Horton, 2000; Gehrels, 1994; Gehrels, 2000). Past sea levels can be reconstructed from salt-marsh sediments by determining their ‘indicative meaning’, i.e. the tidal elevation at which the sediments were originally deposited. This is achieved by relating fossil microfauna in cores to the elevation of the marsh surface where the living counterparts of the microfossils are found. The principle underpinning this methodology and the use of quantitative techniques to determine indicative meaning are appraised at length by Barlow et al. (2013). This study first constructs and then applies a local foraminifera-based transfer function to determine indicative meanings for salt-marsh sediments in a core from Malltraeth marsh.

Forty-eight surface training set samples were taken from the surface of the salt marsh along a 218 m transect spanning from 53°17′72.86″N, 4°38′01.92″W to 53°17′77.49″N, 4°38′30.23″W to construct the transfer function used to reconstruct former relative sea-level changes. 20 Initial reconnaissance cores were collected at 10 m intervals along the same transect with a 20 mm diameter gouge and sediments logged in the field according to Troels-Smith (1955). From this reconnaissance the primary fossil core for further analysis (foraminifera, radiocarbon, particle size (PSA) and loss-on-ignition (LOI)) was taken in the high marsh (at 53°10′39.648″N, 4°22′52.7016″W). The selection of this ‘master’ core was based on the obtaining the thickest salt marsh sequence possible whilst also minimizing compaction issues by avoiding the marsh overlaying the mudflat substrate further seaward (Brain et al. 2012). The fossil core was collected with a 60 mm diameter Eijkelkamp gouge corer to a depth of 80 cm. The upper 65 cm of this core was

the salt marsh sequence and the lower 15 cm the underlying sand layer. A replicate core was taken for ^{210}Pb and ^{137}Cs dating. These cores were removed from the core barrel, wrapped in non-PVC cling film and encased in plastic tubing for transportation. All samples were refrigerated at 4°C until sub sampled for foraminifera and other analyses. Elevations of all field samples were surveyed with a dumpy level to an Ordnance Datum (OD) flush bracket benchmark (S7594) on the south corner of a former church in Malltraeth (53°11′33.468″N, 4°23′7.4796″W).

From the fossil core, 2 ml of sediment was sub-sampled at 1 cm intervals for foraminifera. At 2.5 cm intervals, 3.375 cm^3 sub samples were taken to determine downcore trends LOI and PSA. LOI was performed using a modified Gale and Hoare (1991) method using 5.0±0.10 g, with heating over 24 hours at 430˚C. For PSA, sub-samples were riffled down and treated with 0.1% sodium hexametaphosphate, before dispersal in de-ionized water within the instrument using ultrasound and pumping. Resultant data were used to calculate the mean and median grain size of each sample, as well as sorting, skewness, and probability distribution. PSA samples were then analyzed in a Horiba LA-950 laser diffraction particle size distribution analyzer.

Both surface and fossil foraminifera were sampled and analyzed using the standard techniques of Scott and Medioli (1980). Foraminifera sub-samples were wet-sieved between 500 μm and 63 μm and treated and stored in a rose Bengal 30% ethanol solution to stain living foraminifera and preserve the samples. Foraminifera were identified and wet-picked from a Bergeroff tray under an Olympus SZ61 microscope. Foraminifera taxonomy is based on De Rijk (1995).

Seven 1 cm slice sub-samples samples were taken for bulk radiocarbon at 5 cm, 20 cm, 25 cm 35 cm, 50 cm, 55 cm and 65 cm depth (GR-A-R1 to GR-A-R9). Plant macrofossils would have been preferred but were not found in the decomposed organic sediment. Two further samples were taken at 60 cm depth, one for radiocarbon dating of the humin fraction, and another of plant fragments found at this depth (though this was later determined to likely have been rootlet material).With debris, rootlets and other potentially non-contemporaneous detritus removed, one humin fraction (GR-A-R8), one plant macrofossil (GR-A-R9), and seven bulk (GR-A-R1 to R7) radiocarbon ages were determined by accelerator mass spectrometry (AMS). AMS^{14}C analysis was conducted at the 14CHRONO Centre of Queens University Belfast. Calibration was undertaken using CALIB 7.1 Radiocarbon Calibration software (Stuiver et al. 2018).

The ^{210}Pb sample core (0-30 cm) was chopped into thirty continuous 1 cm slices, freeze dried, weighed and sieved to <2 mm. The <2 mm sediment was homogenized in a Teemer mill. After settling in petri dishes for 21 days to allow for equilibrium to establish between ^{214}Pb, ^{226}Ra and its daughter isotopes, radionuclide activity concentrations were measured using the EG&G Ortec planar (GEM-FX8530-S N-type) HPGe Gamma spectrometer in the Plymouth University Consolidated Radioisotope Facility (CoRIF). Total ^{210}Pb was measured by its gamma emissions at 46.5keV and the supported component calculated by the subtraction of ^{226}Ra activity, which was measured by the gamma emission of ^{214}Pb at 295 and 352 KeV with correction for ^{214}Bi emissions.

The instrument was calibrated using traceable radioactive standard spiked soils provided by AEA Technology Plc. Calibration relationships were obtained using EG&G GammaVision software and verified by comparison tests between laboratories with International Atomic Energy Agency (IAEA) supplied materials.

3.2. Freshwater marsh sea-level reconstruction

Many backbarrier systems in north Wales are closed from the sea and contain deposits of freshwater peat. Gehrels and Anderson (2014) show that these systems can be suitable environments for sea-level reconstructions, provided that the groundwater table was coupled to sea level during the period covered by the sea-level reconstruction. By combining empirical observations with groundwater modelling it is possible to reconstruct Holocene sea-level changes. The procedure for calculating past sea level from freshwater back-barrier peat is described in detail by Gehrels and Anderson (2014) and we follow the same method here.

Groundwater monitoring wells were installed on a transect perpendicular to the barrier, positioned centrally on the marsh. The wells were located at 20 m, 60 m and 90 m. Monitoring was carried out with Aqua TROLL 200 data loggers, which measure fluctuations in temperature, pressure and salinity every 15s. Monitoring was carried out for 32 consecutive months in well 1 and 17 consecutive months for wells 2 and 3.
An Eijkelkamp gouge corer was used to undertake a stratigraphic survey of 36 cores along three shore parallel transects behind the barrier (Fig. 1), providing a picture of the morphology of the valley floor and the stratigraphy of the Holocene infill. A "Russian" chamber corer was used to collect samples for analysis in the laboratory and to obtain samples for radiocarbon dating. For palaeosea-level determinations, the interface between the Holocene base and freshwater peat was sampled in two cores (RC1 and RC2, Fig. 1). Plant macrofossils were sampled from the basal peat samples for ^{14}C dating. AMS ^{14}C analyses were performed by the Natural Environment Research Council (NERC) Radiocarbon Laboratory. Calibration was carried out using CALIB 7.1 (Stuiver et al. 2018) to Cal years BP.

A Trimble R6-3 Differential GPS was used to survey elevations relative to UK Ordnance Datum. A further survey was undertaken to measure the topographic gradient at the edge of the marsh to estimate the gradient in the groundwater in the area where basal peat is formed, following the methods described in Gehrels and Anderson (2014).

4. Results

4.1 Salt-marsh surface foraminifera

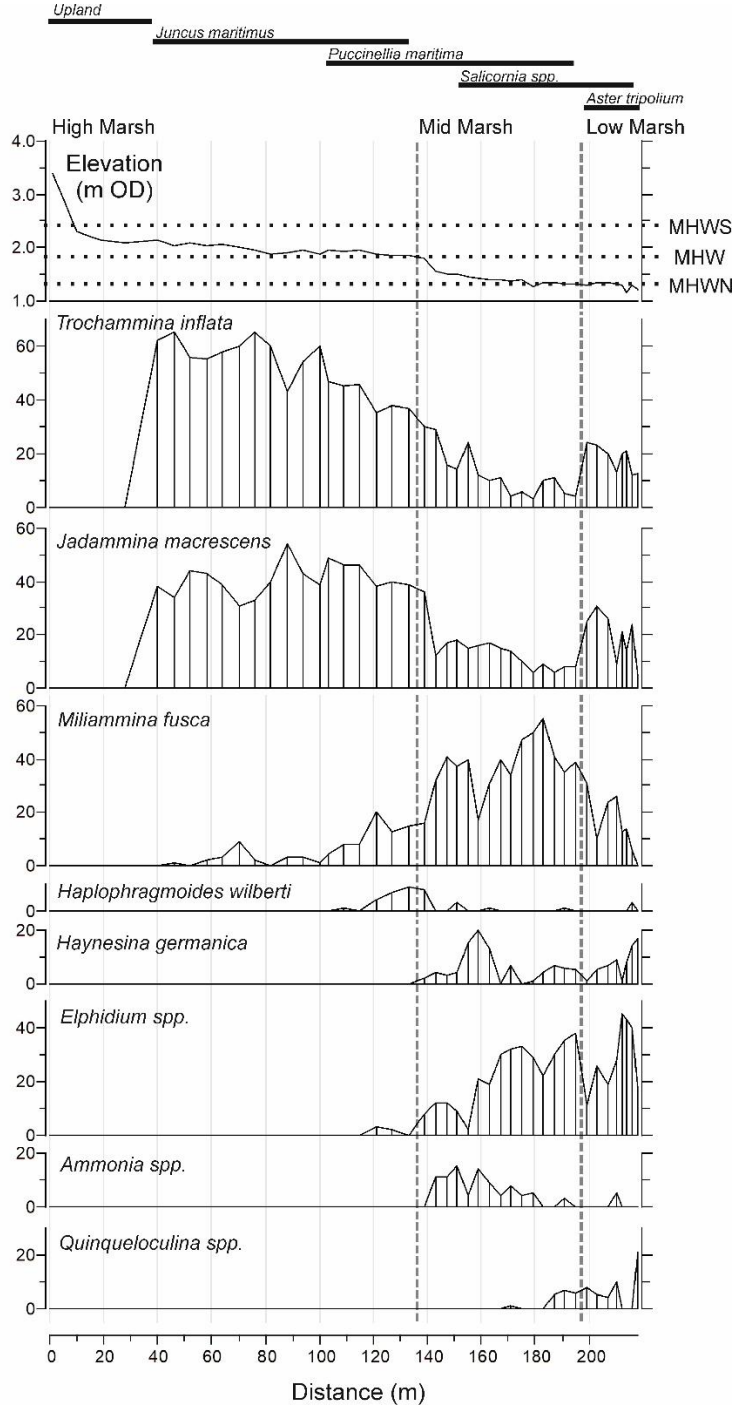

Figure 2. Distribution of surface salt marsh dead foraminifera from original 44 samples, elevation profile, tidal elevations and vegetation zonation. Elevations of mean high water (MHW) of spring (MHWS) and neap (MHWN) tides are shown on elevation profile

The foraminifera across the Malltraeth marsh surface comprise four agglutinated species (Fig. 2.): *Jadammina macrescens, Trochammina inflata, Miliammina fusca* and *Haplophragmoides wilberti*). The calcareous species were grouped into three genera: *Elphidium* including *williamsoni*, and *excavatum*; *Ammonia* consisting of *beccarii* variants; and *Quinqueloculina*. The upper limit of foraminifera on the marsh is at 2.08 m OD.

The marsh exhibits strong zonation in foraminifera along the elevation gradient. The high marsh is dominated entirely by agglutinated species, primarily by *J. macrescens* and *T. inflata*. In the mid marsh *M. fusca* becomes the dominant species with calcareous foraminifera increasing in abundance moving further seaward. Amongst the agglutinated species the relative abundance of *J. macrescens, T. inflata* and *M. fusca* represents the strongest indicator of elevation, with *Haplophragmoides wilberti* primarily occupying a small niche at the boundary of the mid and high marsh zones.

4.2. Salt-marsh litho- and biostratigraphy

The marsh stratigraphy is mostly composed of an organic silt overlying a sand deposit, believed to be of aeolian origin associated with sand from the Newborough dunes, which ranges from 7.5 cm thick at its most seaward to at least 20 cm at its most landward (Fig. 3). Moving seaward this sand is replaced by a sandy clay.

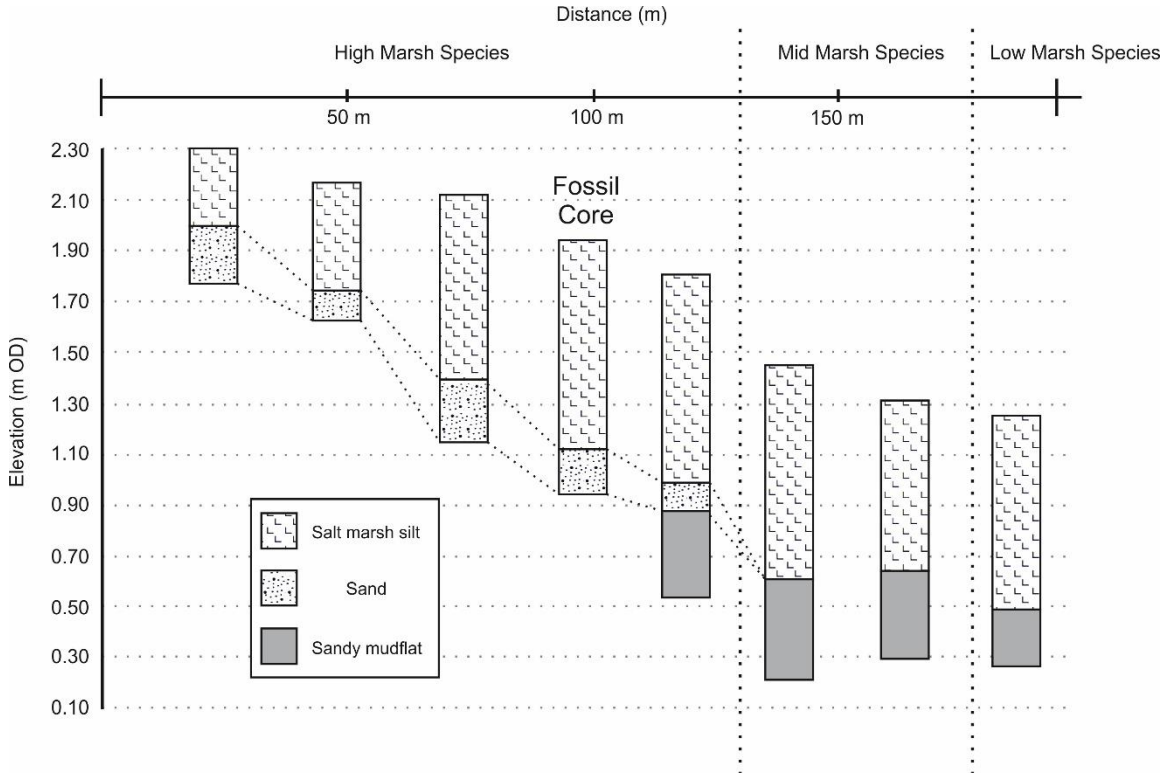

Figure 3. Stratigraphy of Malltraeth Salt Marsh along study transect, landward to seaward

The median particle size in the core (Fig. 4) is dominated by the silt fraction. The sandy substrate is reflected in a sharp increase in median particle size and reduced silt content.

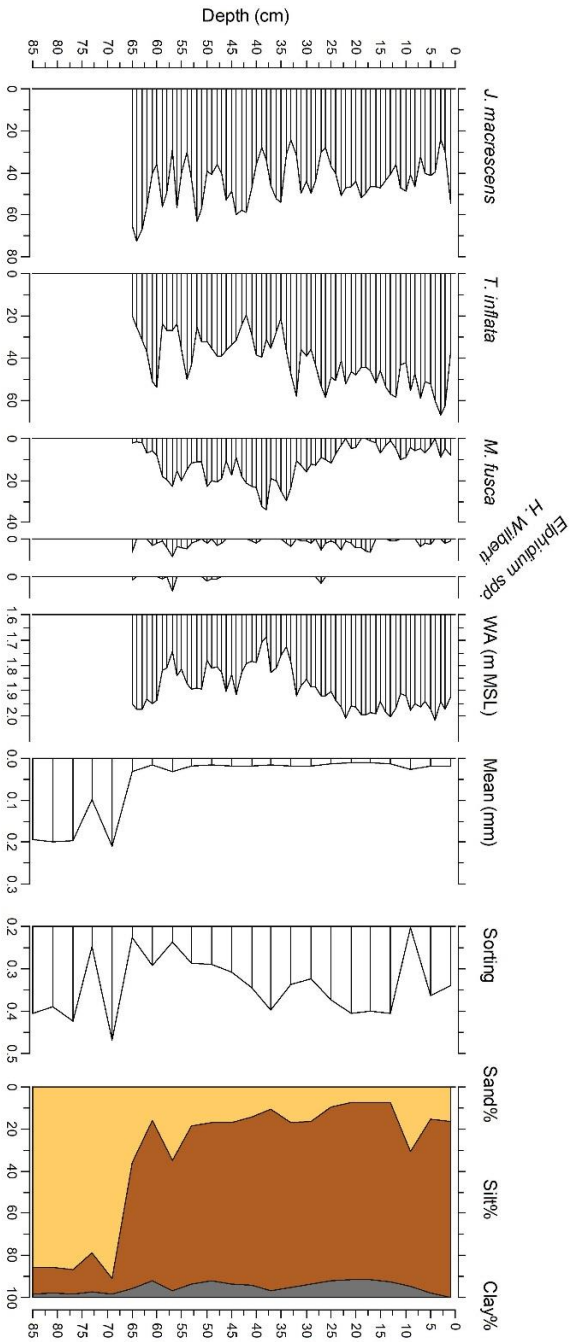

Figure 4. Fossil core dead fossil foraminifera distributions, WA reconstruction and particle size data.

The fossil foraminiferal assemblage consists only of species also found in the modern training dataset and is dominated almost entirely by agglutinated foraminifera, with some incidences of damaged *Elphidium* spp. and *Ammonia* spp. The species distribution in the upper core is representative of its position at the surface slightly above the boundary of the mid and high marsh. The main changes downcore occur in the abundance of *M. fusca* which tends to be more abundant at greater depth. *H. wilberti* is found intermittently throughout the fossil assemblage though always comprises <10% of the assemblage at any given depth. Foraminifera were not found in the underlying sand.

4.3 Salt-marsh chronostratigraphy

Of the nine salt-marsh radiocarbon samples, four (GR-A-R1, R2, R6) returned modern radiocarbon ages (>1950) (Table 1.). These results were therefore separately analyzed by bomb-spike calibration using CALIBomb (Reimer et al. 2004). GR-A-R6 produced ages younger than the overlying GR-A-R2. GR-A-R6 also produced young ages compared to the GR-A-R3 only 5 cm lower in the core. These apparent age reversals may be a result of modern carbon contamination from active root networks, reworking of recent material, or simply an artefact of slow marsh growth in this period. GR-A-R9 yielded a modern age at a depth of 60 cm; it is likely this sample was rootlet material rather than a significant plant macrofossil. The humin fraction sample GR-A-R8 produced an age consistent with the two surrounding bulk samples. Based on these considerations, radiocarbon samples GR-A-R3 and R9 were discarded, leaving seven samples that were used in the calculation of the age-depth model (Fig. 5e).

Table 1. Radiocarbon content reported as $F^{14}C$ as per Reimer et al. (2004) CALIBomb. (Reimer et al. 2004) used to calibrate GR-A-R1, R2, R6. CALIB 7.0 used for all other samples with IntCal13 calibration curve. Samples included in age depth model in bold. CPAV is the Calibration Peak Area Value produced by CALIB 7.0 (Stuiver et al. 2018)

Sample Code	Depth (cm)	Material Type	$F^{14}C \pm 1\sigma$	2σ age range (ka BP)	2σ age range (AD)	CPAV
GR-A-R1	**5 cm**	**Bulk**	**1.0454 ± 0.0034**	**0.0085 – 0.0091** **0.0613 – 0.0615**	**2009 – 2008** **1956 – 1956**	**0.655** **0.345**
GR-A-R2	**20 cm**	**Bulk**	**1.0181 ± 0.0040**	**0.0613 – 0.0628**	**1956 – 1955**	**1.000**
GR-A-R6	30 cm	Bulk	1.1946 ± 0.0051	0.0298 - 0.0334 0.0588- 0.0597	1988 – 1984 1959 - 1958	0.915 0.085
GR-A-R3	**35 cm**	**Bulk**	**0.9153 ± 0.0036**	**0.766 - 0.71** **0.657 - 0.632**	**1252 - 1308** **1361 - 1386**	**0.881** **0.119**
GR-A-R7	**50 cm**	**Bulk**	**0.7675 ± 0.0034**	**2.369 - 2.319** **2.244 - 2.243** **2.228 – 2.066**	**351 – 301 BC** **226 – 225 BC** **210 – 48 BC**	**0.113** **0.001** **0.886**
GR-A-R4	**55 cm**	**Bulk**	**0.7139 ± 0.0031**	**2.933 – 2.824**	**915 – 806 BC**	**1.000**
GR-A-R8	**60 cm**	**Humin Fraction**	**0.6943 ± 0.0031**	**3.248- 3.031**	**1230 – 1013 BC**	**1.000**
GR-A-R9	60 cm	Plant Macrofossil	1.1114 ± 0.0032	0.0228 - 0.0188	1995 - 1999	0.944
GR-A-R5	**65 cm**	**Bulk**	**0.6836 ± 0.0037**	**3.443 – 3.225** **3.155 – 3.153**	**1425 – 1207 BC** **1137 – 1135 BC**	**0.998** **0.002**

The ^{137}Cs depth profile (Fig. 5a) shows increase with depth until 14 cm, reaching a peak at 19 cm. ^{137}Cs values at 17 cm, 18 cm and 19 cm all exist within error of one another presenting some difficulty in determining an exact depth to confidently attribute to the 1963 ^{137}Cs deposition peak. This wide peak may be a result of mobility of ^{137}Cs within the profile (Foster et al. 2006). ^{137}Cs reaches a minimum (17.16 Bq/kg) at 29 cm. Below 30 cm ^{137}Cs once again increases with depth although to levels consistent with the upper 5 cm of the core.

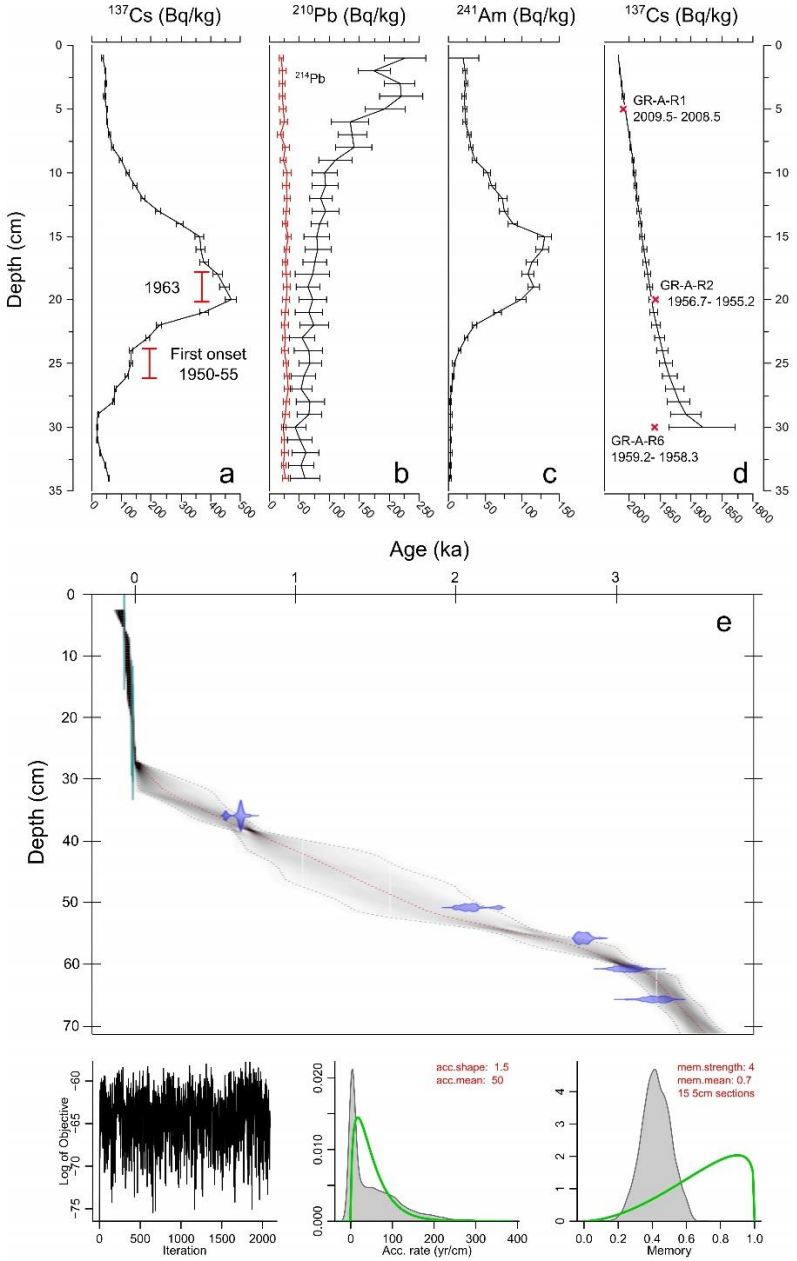

Figure 5. a. Gamma spectrometry results for salt marsh core. a. ^{137}Cs depth profile with suggested age marker and radiocarbon results for comparison, b. ^{210}Pb and ^{214}Pb depth profile, c. ^{241}Am depth profile, d. ^{210}Pb age-depth model derived using CRS model (Appleby, 2001) radiocarbon sample results included for comparison. e. Age-depth model derived using RBacon (Blaauw and Christen, 2011)

Three ^{137}Cs age markers can be used to date sediments: the fallout from the 1986 Chernobyl reactor incident, the 1963 weapons peak, and the first significant environmental presence of this radionuclide around 1950–1955. The 1963 weapons peak may be reasonably interpreted at any depth between 17 cm and 19 cm. This is particularly likely when considered alongside the Am-241 activity, which has notable peaks at 14 cm and 18 cm and is associated with the maximum fallout signal of early 1960s but not of the initial fallout of the 1950s or 1986 (Marshall et al. 2007). Caution should be taken when interpreting ^{241}Am in this way, however, as Plutonium isotopes which were associated with the 1950s and 1986 can also be a primary source of ^{241}Am in modern sediment archives due to the decay of ^{241}Pu with a half-life of 14.4 y (Marshall et al. 2007). The onset of significant environmental radionuclides is also difficult to determine given potential vertical movement of ^{137}Cs although a range of 22 cm to 24 cm is suggested here. There is no clear indication of the 1986 Chernobyl fallout within the profile.

The total ^{210}Pb activity profile broadly demonstrates a typical exponential decay but contains several small peaks (most notably in the upper 7 cm). This uneven decay prevents the use of the Constant Initial Concentration (CIC) model for ^{210}Pb age derivation and the Constant Rate of Supply model (CRS) was used instead (Appleby, 2001).

The depth for A(0) (the total inventory of $^{210}Pb_{xs}$ of the entire core) is usually defined as the point where $^{210}Pb_{xs}$ is at or approximating zero. In this study $^{210}Pb_{xs}$ at no point reaches zero, therefore the minimum value of $^{210}Pb_{xs}$ was used, which occurs at 29 cm. This A(0) is justified in the context of the ^{137}Cs data as this value placed the year 1963 at 18 cm depth. Bomb-spike calibrated radiocarbon samples GR-A-R1 and R2 are consistent with the age depth model produced from the ^{210}Pb. GR-A-R6, however, is 60 years younger than the age suggested by the ^{210}Pb and plots outside the ^{210}Pb error margin. This further reinforces the likelihood that GR-A-R6 is anomalous and should be discarded.

The age-depth model of the core (Fig. 5e) was derived using Bacon in the statistical computing environment R (Blaauw and Christen, 2011). The methodology is based on controlling core accumulation rates using a gamma autoregressive semiparametric model with an arbitrary number of subdivisions along the sediment. Greater detail on the statistical model used in available in Blaauw and Christen, (2011). The model was run with a section thickness of 5 cm (res=5) and a memory strength of 4 (mem. strength= 4). This age depth model was produced using radiocarbon samples GR-A-R1, R2, R3, R4, R5, R7, R8 and the inferred 1963 and 1950-55 ^{137}Cs age markers. The ^{210}Pb model was excluded from the final age-depth model as this results in artificially inflating the precision of the final model at these depths, as per Kemp et al. (2013). Due to the lack of ages between 35 cm and 50 cm depth, uncertainty is high between 40- 45 cm, therefore caution should be taken with interpretation of sea-level reconstruction results between 0.5 ka and 2 ka BP.

4.4. Transfer function and sea-level derivation

Surface-foraminifera distributions (Fig 2.), plus four additional samples taken to target elevations not covered by the original transect (SURF-45 to -48 at 1.66, 1.71, 1.79, and 1.83 m OD), were used as the training set informing the transfer function. Calcareous foraminifera were eliminated from the training set because of their usual dissolution upon burial in salt-marsh sediment (Gehrels, 2000). The eight most seaward samples (SURF-1 to -9) were excluded from the transfer function as they comprised almost entirely of calcareous species and produced residuals >0.2 m when included. The four most landward samples (SURF-40 to 44) were also excluded as they contained few intact foraminifera (<10), likely due to their proximity to the upper vertical limit of salt marsh foraminifera. In total, 36 samples inform the transfer function.

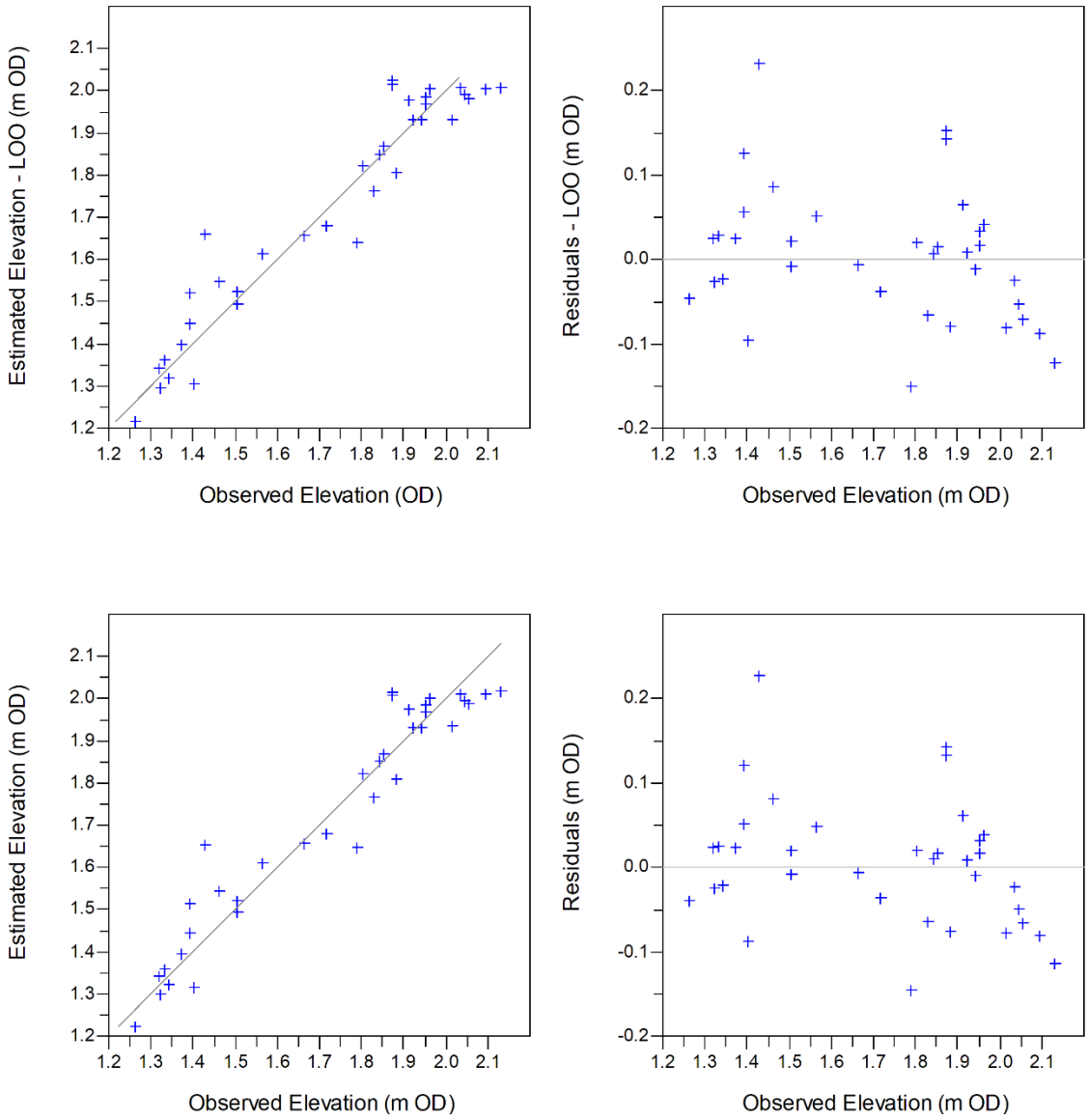

Figure 6. Relationship between predicted and observed elevations for chosen first component of transfer function created using WA with leave-one-out cross validation

Table 2. Model performance for transfer function components

Component	R^2	RMSE	RMSEP	%Change
Component 1	0.93	0.08	0.08	...
Component 2	0.93	0.07	0.08	-2.2
Component 3	0.93	0.07	0.08	0.04

The transfer function was produced using a weighted averaging partial least-squares (WA-PLS) technique using the C2 program (Juggins, 2003). WA-PLS is the most widely used approach for unimodal species-environment responses (Barlow et al. 2013). C2 model performance is assessed by a coefficient of determination (R^2), an apparent root mean square error (RMSE) and a root mean square error of prediction (RMSEP) a value which represents maximum bias (Gehrels, 2000). The RMSEP was produced using a leave-one-out jack-knifing approach and is considered the strongest indicator of the predictive strength of the transfer function. The transfer function performance is presented in Fig. 6 and a statistical summary is presented in Table 2. The relationship between observed and foraminifera-predicted elevation (Fig. 6) is very strong, indicating the excellent performance of the transfer function ($R^2 = 0.92$ for Component 1). These results suggest the transfer function is suitable for application to reconstructing past sea levels.

The transfer function's first component was chosen for sea-level analysis as subsequent components did not produce RMSEP values >5% greater as per Barlow et al. (2013). The sea level parameters derived from the age-depth model (Fig. 5e) and indicative meaning predictions of the transfer function can be found in the supplementary information. Also shown are the results of a modern analogue technique (MAT) which was used quantify the similarity of each fossil sample to its nearest modern analogue. All fossil samples were found to have a "close" modern analogue (20th percentile of similarity according to Watcham et al. (2013). None reached the "good" threshold of the 5th percentile but 54 of 65 fossil samples were within the 10th percentile.
Sea level (SL) is calculated by subtracting the indicative meaning predictions of the transfer function (I) from the elevation of each core sample (E). The results of the full late Holocene sea level reconstruction are also presented in Fig. 8a. Typically it is necessary to determine a compaction error component for such a reconstruction (Brain et al. 2012). However, as the salt marsh data in Fig. 8a shows a good fit with the basal SLIP RC1 we suggest that the compaction component is likely negligible and opt to use the transfer function's RMSEP for 2σ as our standard error margin of +/- 0.16 m.

4.5. Rhoscolyn sea-level index points

At Rhoscolyn the stratigraphy of the back-barrier marsh consisted of *Phragmites* peat overlying woody peat deposits which vary from 2 cm to 2 m in thickness (Fig. 7). The site is a closed back-barrier freshwater transgressive system (Kraft and Chrzastowski

1985). In a closed system, the rollover of the barrier results in onshore migration: a *Phragmites* swamp replaces the carr as groundwater rises in response to changing hydraulic gradients, driven by RSL rise. As such it is reasonable to expect the carr or fen peat was deposited at the leading edge of the Holocene transgression and can be expected to represent an archive of past sea-level rise (Gehrels and Anderson, 2014). The stratigraphy contained a large sand deposit in transect Y-Y[1], which was interpreted as an overwash deposit based on its geometry.

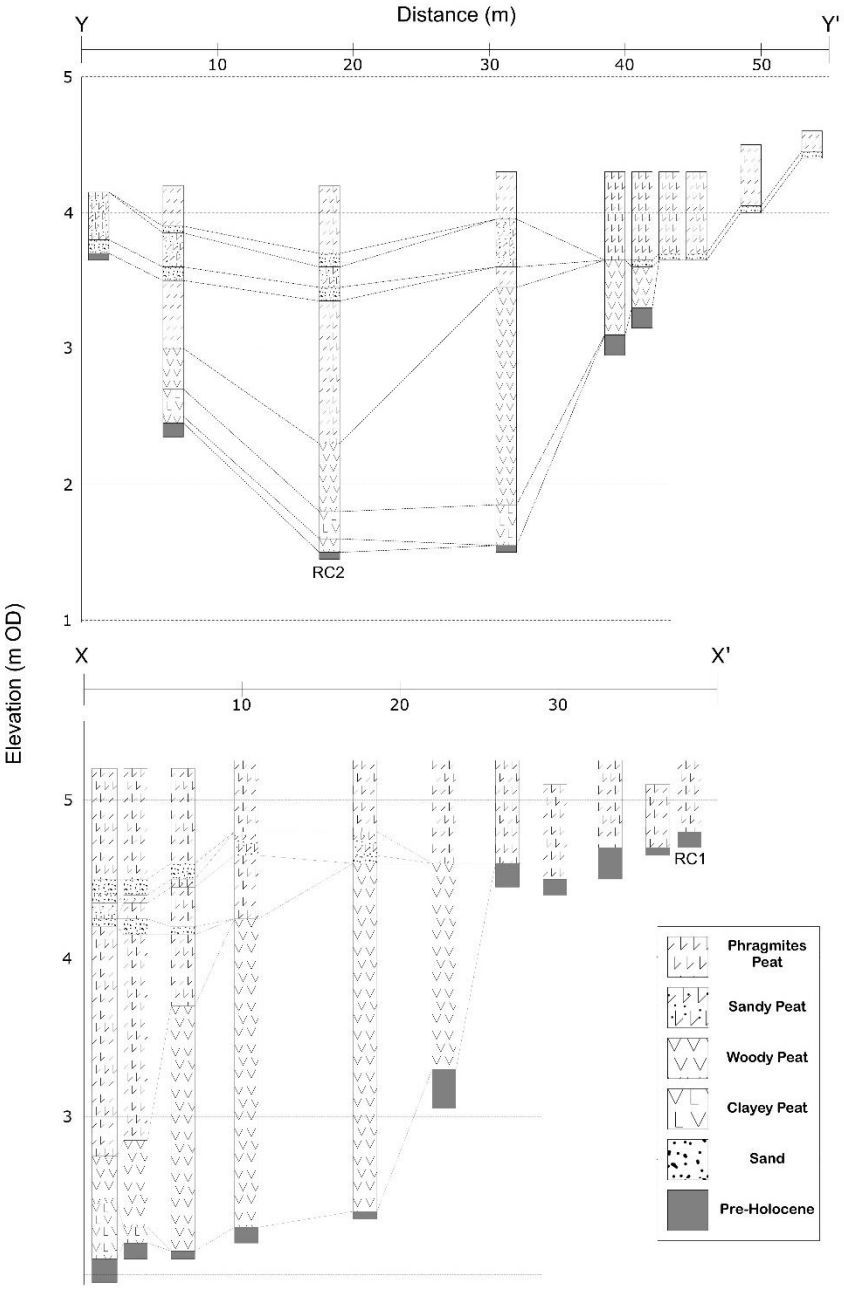

Figure. 7. Stratigraphy of Rhoscolyn freshwater back-barrier marsh. Transects run west to east.

For coastal freshwater back-barrier wetlands to be suitable archives of sea-level data, it is necessary to demonstrate a link between tidal and ground water oscillations. Wavelet coherence analysis was applied to the tide-gauge and groundwater well data, using a Matlab script made available by Grinsted et al. (2004). This enabled the simultaneous analyses of two time-series to examine relationships between the signals in time frequency space. A three-step approach was taken to analyze the data. First, a continuous wavelet transform (CWT) was applied to both datasets, before applying a cross wavelet transform (XWT) to test for significant power correlations in the signal. Finally, the coherence of the wavelets in time frequency space was tested for significance. All significance tests were against red noise, using Monte Carlo methods.
Wavelet analyses, using the technique presented by Grinsted et al. (2004) provides a robust insight into the tidally induced groundwater oscillations. Cross wavelet power highlights periods that share a high power signal for a particular time period. This is clearly identifiable in the wavelet analyses for the semi-diurnal tide and shows the tidal and groundwater signals are slightly out of phase with each other, which is to be expected as the tidal signal takes time to propagate through the barrier. The power of wavelet analyses enables a clear identification of a tidal signal in the groundwater, at greater distances than is possible using Fast Fourier Transform based spectral analyses. Groundwater monitoring shows a significant relationship, using Monte Carlo methods, between groundwater oscillations and the tidal movements of the sea. The groundwater is sensitive enough to oscillate in correlation to the semi-diurnal tide. The signal remains consistent through the sandy barrier at Rhoscolyn and show that that the groundwater height in the backbarrier, and thus peat formation, is controlled by sea level (Gehrels and Anderson 2014).

The procedure for calculating past sea level from freshwater back-barrier peat is described by Gehrels and Anderson (2014) and the same method is followed here. The reconstruction of past mean sea level, from basal peat, follows the relationship $SL = E - I$, where E is the elevation of the sample and I is the indicative meaning. The determination of I is complicated by the existence of a gradient in the groundwater. As our sample formed a distance behind the barrier, we must correct for the influence of the gradient. As such, we calculate an original past mean sea level from $SL = E - I - GW$, where GW is the correction for the groundwater gradient.

The groundwater gradient was estimated by measuring the topography along the edge of the marsh, where it formed against the valley edge, as it is the modern day analogue to where the basal peats formed. The gradient of 0.47 ± 0.04 m per 100 m, and the fact that sea level was lower in the past, necessitate a calculation of the distance between the present-day location of the samples and the original position of the palaeobarrier further seaward at the time the basal peat formed.

Landward barrier migration is a result of relative sea-level rise and can be calculated as a function of offshore gradient from $R=1/\tan\theta\ S$ (Bruun, 1962). The original indicative meaning was taken as the average height of peat formation directly behind the barrier. From this, the estimated past sea level was used to calculate the offshore distance of the palaeobarrier. This process was repeated iteratively, until there was no variation in

indicative meaning for three iterations (Table 3). Vertical error was calculated by running these iterations for two standard deviations in the groundwater gradient estimations. Using radiocarbon results and SLIP parameters shown in Table 4, RC1 and RC2 are plotted in Fig. 8a and 8c. The RC1 Late Holocene basal sample provides a SLIP younger than any in the current north Wales database (Shennan et al. 2018) at 1.9 ka BP and -0.33 m lower than present day. The RC2 Holocene basal SLIP is in good agreement with the existing SLIPs of Bedlington (1993), Heyworth and Kidson (1982), and Roberts et al. (2011), indicating a sea level -5.49 m at c. 7.4 ka BP (Fig. 8c).

Table 3. Groundwater Model Iterations

Iteration		RC1	RC2
	Height (m OD)	5.19	4.19
	Depth (m)	0.49	2.65
	Sample Height (m OD)	4.70	1.54
	Initial Indicative Meaning (m OD)	4.90	4.90
1	Shore Distance (m)	67.00	23.00
	IM Correction	0.31	0.11
	Sea level	-0.51	-3.47
2	Shore Distance (m)	42.55	286.61
	IM Correction	0.20	1.35
	Sea Level	-0.40	-4.71
3	Shore Distance (m)	33.06	388.99
	IM Correction	0.16	1.83
	Sea Level	-0.36	-5.19
4	Shore Distance (m)	29.37	428.76
	IM Correction	0.14	2.02
	Sea Level	-0.34	-5.38
5	Shore Distance (m)	27.93	444.21
	IM Correction	0.13	2.09
	Sea Level	-0.33	-5.45
6	Shore Distance (m)	27.38	450.21
	IM Correction	0.13	2.12
	Sea Level	-0.33	-5.48
7	Shore Distance (m)	27.16	452.54
	IM Correction	0.13	2.13
	Sea Level	-0.33	-5.49
8	Shore Distance (m)		453.44
	IM Correction		2.13
	Sea Level		-5.49
9	Shore Distance (m)		453.79
	IM Correction		2.13
	Sea Level		-5.49

Table 4. SLIP parameters for Rhoscolyn freshwater samples.

Index Point	Age (Ka BP)	Error +	Error -	RSL	RSL +error	RSL - error
RC1	1.87	2.32	1.87	-0.33	0.04	0.05
RC2	7.38	7.45	7.37	-5.49	0.81	0.48

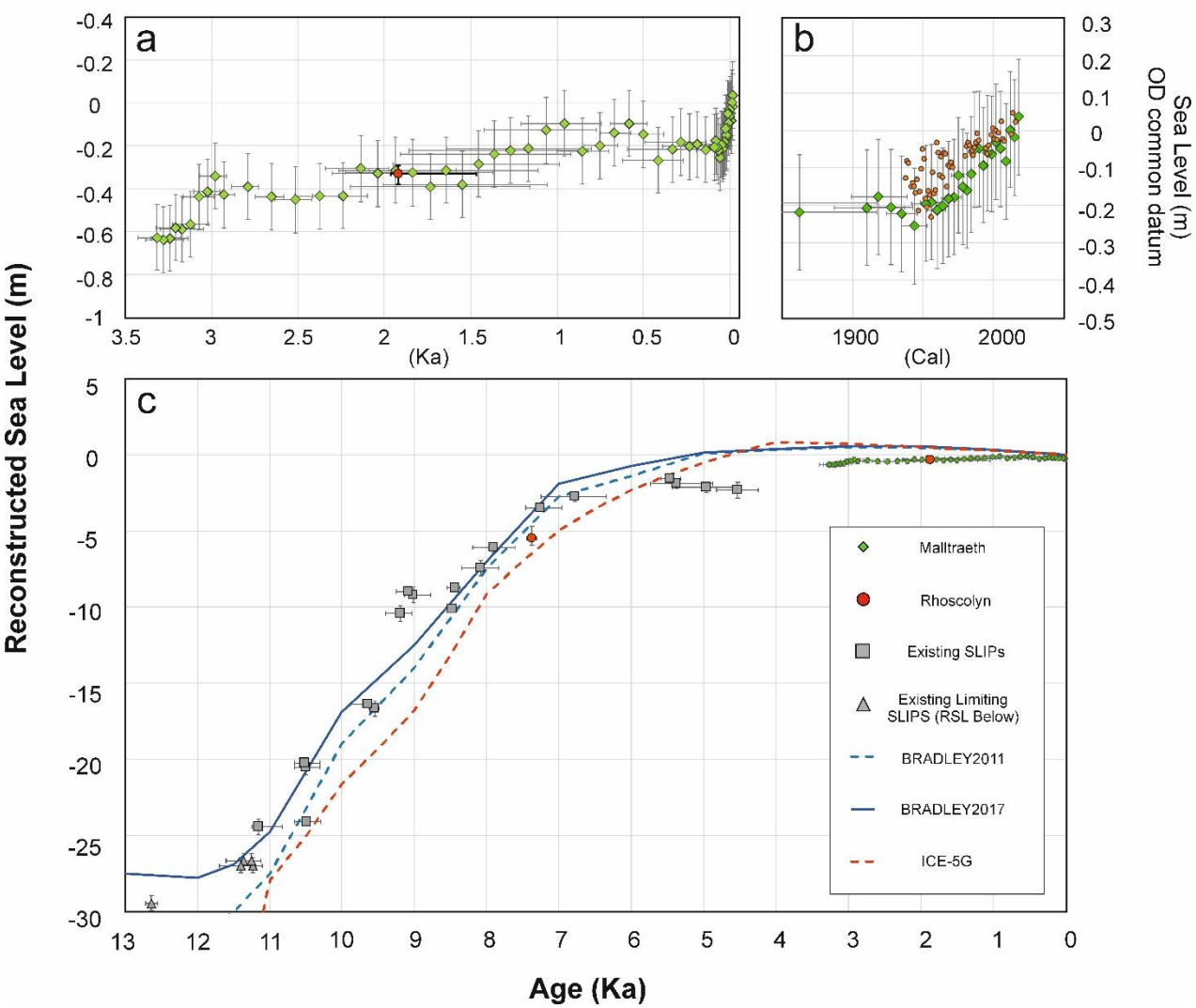

Figure 8. a. Late Holocene sea-level history for north Wales derived from Malltraeth Marsh. Red dot freshwater sample RC1. b. Post-industrial sea-level acceleration in Malltraeth. Orange data from Holyhead tide gauge. c. Holocene relative sea-level changes in north Wales, compared with GIA models (Bradley et al 2011; Peltier 2004; Shennan et al. 2018)

5. Discussion

The RSL record derived from 24 SLIPs and the Late Holocene salt-marsh for north Wales (Fig. 8c) show that relative sea level rose ~0.65 m in the last 3,300 years and has now reached its highest level in the Holocene. Post-industrial acceleration of sea-level rise is evident in the Malltreath data (Fig. 8a) and begins in the early to mid-20th century. The salt-marsh reconstruction matches with the lower limit of the tide-gauge data.

In North Wales relative sea level rose ~30 m over the course of the Holocene. The data suggest that sea-level rise was fairly linear between 12 ka BP and 7 ka BP at a rate of ~5.3 m ka^{-1}. There is nothing in the data to suggest that sea level was at any point > 0 m after 7 ka BP. Although there is some suggestion for a relative sea-level stability between 6-4 ka BP, or even potentially a small sea-level fall, the vertical uncertainty of the individual SLIPs prevents attaching any great significance to this. It is clear, however, that our new Late Holocene relative sea-level data leave no room for a Mid-Holocene relative sea-level highstand in north Wales.

The Holocene RSL reconstruction is compared with data produced by two GIA models presented in Shennan et al. (2018) (BRADLEY2011 and BRADLEY2017) and with predictions from the ICE5G model (Peltier, 2004). The BRADLEY2011 and BRADLEY2017 models predict sea level well between 12 ka BP and 7 ka BP. The prediction from BRADLEY2017 is slightly closer to the empirical data and produces sea levels greater than the limiting SLIPs between 13 and 11 ka BP, whereas BRADLEY2011 underestimates sea level in this period. This improvement likely stems from the higher grid resolution of ~35 km in BRADLEY2017 compared to ~70 km in BRADLEY2011 (Shennan et al. 2018). Both BRADLEY models presented in Shennan et al. (2018) overestimate sea level in the Mid- and Late Holocene, reaching a highstand at 5 ka BP and predicting Late Holocene sea levels >0 m. ICE5G has a poor fit to the entire empirical dataset, underpredicting sea level prior to 7 ka BP and overestimating after 5 ka BP. It also predicts a larger highstand than either BRADLEY model.

The differences between these models may be a result of the different way the ICE-5G (and its subsequent iterations) and the BRADLEY models handle the rate of global ice melt in the Mid Holocene. ICE-5G and 6G (Argus et al. 2014) infer a slowdown in global melt rate ~ 8 ka BP, a ~4m (ICE-5G) and ~2m (ICE-6G) equivalent sea level rise (ESL: the spatially uniform sea-level change from mass exchange between the ice sheets and the oceans (Farrell and Clark, 1976)) between 7 and 4 ka BP, and no melt subsequent to 4 ka BP (Bradley et al. 2016). The BRADLEY models assume that the slowdown of ESL started later (~7 ka BP) and that melt also ended later (Bradley et al. 2016). This can have the effect of "drowning" Mid Holocene highstands with greater Late Holocene contributions. For the regional BRADLEY models, it may also be a result of incorrect estimation of isostatic change for the Holocene, or, perhaps most likely, a composite of these effects. Attributing a cause to this mismatch is complicated by a general GIA modelling problem, that many possible variables in the Earth-model can provide similar predictions with equally good fit to the empirical data (Stockamp et al. 2016). Despite the closer fit of the BRADLEY models to the geological data it is clear there is still need for

further refinement of model parameters to successfully match this region's relative sea-level data with GIA model predictions, particularly for the Mid- to Late Holocene.

The false predictions of a Mid-Holocene highstand and overestimation of Late Holocene sea level has implications for GIA model and sea-level predictions for the UK. This is particularly true if these differences stem from errors in determination of regional scale isostatic adjustment, as accurate models of future isostatic adjustment are vital in predicting future relative sea level changes, particularly in regions where isostatic contributions are a dominant factor, such as south-west England (Gehrels et al. 2011). Further work from the Britice-Chrono project may help to better resolve the British-Irish Ice Sheet, and its isostatic contributions, and enable the reduction in misfits during the Late Holocene, particularly if it is able to better resolve the Irish Sea Ice Stream (Clark et al. 2018, Small et al. 2018).

6. Conclusions

1. A continuous record of relative sea-level changes during the past 3,300 years were successfully reconstructed from Malltreath marsh, providing the first high resolution data for the Late Holocene in north Wales.
2. The methodology put forward by Gehrels and Anderson (2014) was applied to back barrier freshwater peat at Rhoscolyn to obtain two additional Mid- to Late Holocene sea-level index points for north Wales.
3. By combining the Late Holocene salt-marsh data and freshwater sea-level data with previously published sea-level index points a more complete Holocene relative sea-level reconstruction for north Wales is presented.
4. There is no evidence in the sea-level reconstruction to suggest the existence of a Mid-Holocene highstand in north Wales.
5. There is a need for further refinement of GIA model parameters for the Mid- to Late Holocene to obtain a better fit between GIA model predictions and Holocene relative sea-level reconstructions for north Wales.
6. Such improvements will increase the capability of GIA models to predict more reliably future relative land- and sea levels around the British Isles.

Acknowledgements

Rushby and Richards were supported in their PhD studies by the NERC Doctoral Training Partnership ACCE (Adapting to the Challenges of a Changing Environment) (NE/L002450/1). This study was supported by the NERC Radiocarbon Facility (allocation 2035.1016) for Rhoscolyn ^{14}C samples. ^{14}C samples for Malltraeth were paid for by the Sheffield Luminescence Laboratory.

References

Appleby PG. (2001) Chronostratigraphic Techniques in Recent Sediments. In: Last WM and Smol JP (eds) Tracking environmental change using lake sediments. 2. Physical and geochemical methods. 171-203.

Argus, DF., Peltier, WR., Drummond, R., Moore, AW. 2014. The Antarctica component of postglacial rebound model ICE-6G_C (VM5a) based on GPS positioning, exposure age dating of ice thicknesses, and relative sea level histories. Geophysical Journal International. 198: 537-563

Barlow NL, Long AJ, Saher MH, Gehrels WR, Garnett MH, Scaife RG. (2014) Salt-marsh reconstructions of relative sea-level change in the North Atlantic during the last 2000 years. Quaternary Science Reviews 99: 1-16.

Barlow NL, Shennan I, Long AJ, Gehrels WR, Saher MH, Woodroffe SA, Hillier C. (2013) Salt marshes as late Holocene tide gauges. Global and Planetary Change 106: 90-110.

Bedlington DJ. (1994) Holocene sea-level changes anad crustal movements in North Wales and Wirral. University of Durham.

Blaauw M and Christen JA. (2011) Flexible paleoclimate age-depth models using an autoregressive gamma process. Bayesian Analaysis 6: 4 57-474.

Bradley SL, Milne GA, Shennan I, Edwards R. (2011) An improved glacial isostatic adjustment model for the British Isles. Journal of Quaternary Science 26: 541-552.

Bradley SL, Milne GA, Teferle FN, Bingley RM, Orliac EJ. (2009) Glacial isostatic adjustment of the British Isles: new constraints from GPS measurements of crustal motion. Geophysical Journal International 178: 14–22.

Bradley, SL., Milne, GA., Horton, BP., Zong, Y. (2016) Modelling sea level data from China and Malay-Thailand to estimate Holocene ice-volume equivalent sea level change. Quaternary Science Reviews. 137: 54-68

Brain MJ, Long AJ, Woodroffe SA, Petley DN. Milledge DG, Parnell AC. (2012) Modelling the effects of sediment compaction on salt marsh reconstructions of recent sea-level rise. Earth and Planetary Science Letters 345-348: 180-193.

Brooks AJ, Bradley SL, Edwards RJ, Milne GA, Horton B, Shennan I. (2008) Postglacial relative sea-level observations from Ireland and their role in glacial rebound modelling. Journal of Quaternary Science 23: 175-192.

Bruun P. (1962) Sea-level rise as a cause of shore erosion. Journal of the Waterways and Harbors Division 88: 117-132.

Clark, CD. Ely, JC. Greenwood, SL. Hughes, ALC. Meehan, R. Barr LD., Bateman, MD. Bradwell, T. Doole, J. Evans, DJA. Jordan, CJ, Monteys, X. Pellicer, XM. Sheehy, M. (2018). BRITICE Glacial Map, version 2: a map and GIS database of glacial landforms of the last British–Irish Ice Sheet. Boreas. 47: 11-27

Clout HD. (2007) Contemporary Rural Geographies : Land, Property, and Resources in Britain : Essays in Honour of Richard Munton. London: Routledge.

Collins A and Buchan C. (2004) Provenance and age constraints of the South Stack Group, Anglesey, UK: U–Pb SIMS detrital zircon data. Journal of the Geological Society 161: 743–746.

De Rijk S. (1995) Agglutinated Foraminifera as Indicators of Salt Marsh Development in Relation to Late Holocene Sea Level Rise (Great Marshes at Barnstable, Massachusetts), Utrecht: Febo.

Edwards RJ and Horton BP. (2000) Reconstructing relative sea-level change using UK salt-marsh foraminifera. Marine Geology 168.

Edwards RJ, Wright AJ and van de Plassche O. (2004) Surface distributions of salt-marsh foraminifera from Connecticut, USA: modern analogues for high-resolution sea level studies. Marine Micropaleontology 51: 1-21.

Farrell, WE., Clark, JA. (1976) Postglacial sea-level. Geophysical Journal of the Royal Astronomical Society. 46, 647-667

Foster I, Mighall T, Proffitt H, Walling DE, Owens, PN. (2006) Post-depositional ^{137}Cs Mobility in the Sediments of Three Shallow Coastal Lagoons, SW England. Journal of Paleolimnology 35: 881-895.

Gale SJ and Hoare PG. (1991) Chemical Composition and Analysis. Quaternary Sediments. Chichester and New York: Wiley, 262-265.

Gehrels WR and Anderson WP. (2014) Reconstructing Holocene sea-level change from coastal freshwater peat: A combined empirical and model-based approach. Marine Geology 353: 140-152.

Gehrels WR. (1994) Detrmining Relative Sea-Level Change from Salt-marsh Foraminifera and Plant Zones on the Coast of Maine, U.S.A. Journal of Coastal Research 10: 990-1009.

Gehrels WR. (2000) Using forminiferal transfer functions to produce high-resolution sea-level records from salt-marsh deposits, Maine, USA. The Holocene 10: 367-376.

Gehrels WR. (2010) Late Holocene land- and sea-level changes in the British Isles: Implications for future sea-level predictions. Quaternary Science Reviews 29(13): 1648-1660

Gehrels, WR. Dawson, DA. Shaw, J. Marshall, WA. (2011) Using Holocene relative sea-level data to inform future sea-level predictions: An example from southwest England. 78(3-4): 116-126

Grinsted, A., Moore, JC., Jevrejeva, S. (2004) Application of the cross wavelet transform and wavelet coherence to geophysical time series. Nonlinear Processes in Geophysics. 11:561-566.

Hassani H, Covey-Crump SJ and Rutter EH. (2004) On the structural age of the Rhoscolyn antiform. Geological Journal 39: 141–156.

Heyworth A and Kidson C. (1982) Sea-level changes in southwest England and Wales. Proceedings of the Geologists' Association 93: 91-111.

Horak JM, Evans JA. (2011) Early Neoproterozoic limestones from the Gwna Group, Anglesey. Geological Magazine 148(1): 78-88

Horton BP, Edwards RJ and Lloyd JM. (1999) UK intertidal foraminiferal distributions: implications for sea-level studies. Marine Micropaleontology 36: 205-223.

Juggins S. (2003) User Guide C2, Software for Ecological and Palaeoecological Data Analysis and Visualisation, User Guide Version 1.3, Newcastle: Department of Geography.

Kemp AC, Horton BP, Vane CH, Bernhardt CE, Corbett DR, Engelhart SE, Anisfeld SC, Parnell AC, Cahill N. (2013) Sea-level change during the last 2500 years in New Jersey, USA. Quaternary Science Reviews 81: 90-104

Kopp RE, Kemp AC, Bittermann K, Horton BP, Donnelly JP, Gehrels WR, Hay CC, Mitrovica JX, Morrow ED, Rahmstorf S. (2016) Temperature-driven global sea-level variability in the Common Era. Proceedings of the National Academy of Sciences 113: E1434.

Kraft, JC., Chrzastowski, MJ. (1985) Coastal stratigraphic sequences. Coastal Sedimentary Environments. P625-663.

Lambeck K. (1996) Glaciation and sea-level change for Ireland and the Irish Sea since Late Devensian/Midlandian time. Journal of the Geological Society 153: 853.

Lisle RJ. (1988) Anomalous vergence patterns on the rhoscolyn anticline, anglesey: Implications for structural analysis of refolded regions. Geological Journal 23: 211–220.

Lloyd JM, Zong Y, Fish P, Innes, JB. (2013) Holocene and Lateglacial relative sea-level change in north-west England: implications for glacial isostatic adjustment models. Journal of Quaternary Science 28: 59-70.

Marshall WA, Gehrels WR, Garnett MH, Freeman SPHT, Maden C, Xu S. (2007) The use of‘ bomb spike’ calibration and high-precision AMS 14C analyses to date salt-marsh sediments deposited during the past three centuries. Quaternary Research 68: 325-337.

Milne GA, Shennan I, Youngs BAR, Waugh AI, Teferle FN, Bingley RM, Bassett SE, Cuthbert-Brown C, Bradley SL. (2006) Modelling the glacial isostatic adjustment of the UK region. Philosophical Transactions of the Royal Society A: Mathematical, Physical and Engineering Sciences 364: 931-948.

Packham JR and Liddle MJ. (1970) The Cefni Salt Marsh Anglesey and its recent development. Field Studies 3: 331-356.

Patterson RT, Roland Gehrels W, Belknap DF, Dalby AP. (2004) The distribution of salt marsh foraminifera at Little Dipper Harbour New Brunswick, Canada: implications for development of widely applicable transfer functions in sea-level research. Quaternary International 120: 185-194.

Peltier WR. (1994) Ice Age Paleotopography. Science 265: 195.

Peltier WR. (2002) Global glacial isostatic adjustment: palaeogeodetic and space-geodetic tests of the ICE-4G (VM2) model. Journal of Quaternary Science 17: 491-510.

Peltier WR. (2004) GLOBAL GLACIAL ISOSTASY AND THE SURFACE OF THE ICE-AGE EARTH: The ICE-5G (VM2) Model and GRACE. Annual Review of Earth and Planetary Sciences 32: 111-149.

Prince HE. (1988) Late-glacial and Post-glacial sea-level movements in North Wales with particular reference to the techniques for the analysis and interpretation of unconsolidated estuarine sediments.: University of Wales, Aberystwyth.

Reimer, PJ., Brown, TA., Reimer, RW. (2004) Discussion: Reporting and Calibration of Post-Bomb 14C Data. Radiocarbon, 46(1): 1299-1304

Rhind PM, Blackstock TH, Hardy HS, Jones, RE. Sandison, W. (2001) The evolution of Newborough Warren dune system with particular reference to the past four decades, Liverpool: Liverpool Univ Press.

Roberts MJ, Scourse JD, Bennell JD, Huws, DG. Jago CF. Long BT. (2011) Late Devensian and Holocene relative sea-level change in North Wales, UK. Journal of Quaternary Science 26: 141-155.

Roe HM, Doherty CT, Patterson RT, Swindles, GT. (2009) Contemporary distributions of saltmarsh diatoms in the Seymour– Belize Inlet Complex, British Columbia, Canada: implic ations for studies of sea-level change. Marine Micropaleontology 70: 134-150.

Scott DBM, F S. (1980) Quantitative studies of marsh foraminiferal distributions in Nova Scotia : implications for sea level studies, Washington, D.C. : Cushman Foundation for Foraminiferal Research.

Scott DS and Medioli FS. (1978) Vertical zonations of marsh foraminfera as accurate indicators of former sea-levels. Nature 272: 528-531.

Shennan I, Bradley S, Milne G, Brooks, A. Bassett, S. Hamilton, S. (2006) Relative sea-level changes, glacial isostatic modelling and ice-sheet reconstructions from the

British Isles since the Last Glacial Maximum. Journal of Quaternary Science 21: 585-599.

Shennan I, Bradley SL and Edwards R. (2018) Relative sea-level changes and crustal movements in Britain and Ireland since the Last Glacial Maximum. Quaternary Science Reviews 188: 143-159.

Shennan I, Milne G, Bradley S, (2012) Late Holocene vertical land motion and relative sea-level changes: lessons from the British Isles. Journal of Quaternary Science 27(1): 64-70

Simon KM, Riva REM, Kleinherenbrink M, Frederikse, T. (2018) The glacial isostatic adjustment signal at present day in northern Europe and the British Isles estimated from geodetic observations and geophysical models. Solid Earth 9: 777-795.

Small, D. Clark, CD. Chiverrell, RC. Smedley, RK. Bateman, MD. Duller, GAT. Ely, JC. Fabel, D. Medialdea, A. Moreton, SG. (2017) Devising quality assurance procedures for assessment of legacy geochronological data relating to deglaciation of the last British-Irish Ice Sheet. Earth-Science Reviews. 164: 232-250

Stockamp J, Bishop P, Li Z, Petire EJ, Hansom J, Rennie A. (2016) State-of-the-art in studies of glacial isostatic adjustment for the British Isles: a literature review. Earth and Environmental Science Transactions of the Royal Society of Edinburgh 106: 145-170

Stuiver M, Reimer PJ and Reimer RW. (2018) CALIB 7.1 [WWW program] at http://calib.org.

Troels-Smith J. (1955) Characterisation of unconsolidated sediments. Danmarks Geologiske Undersøgelse 4: 1–73.

Uehara K, Scourse JD, Horsburgh KJ, Lambeck, K. Purcell, AP. (2006) Tidal evolution of the northwest European shelf seas from the Last Glacial Maximum to the present. Journal of Geophysical Research: Oceans 111.

Watcham, EP., Shennan, I., Barlow, NLM. (2013) Scale considerations in using diatoms as indicators of sea-level change: lessons from Alaska. Journal of Quaternary Science. 28(2): 165-179.

Supplementary Material

S1. WA sea level reconstruction parameters

Code	Elevation (m OD) **E**	Age (Ka BP)	Age Min (Ka BP)	Age Max (Ka BP)	Age (Cal. Y)	WA (m MSL) **I**	Sea Level (m) **E-I**	MAT DC. (MAT)
Core-1	1.96	-0.068	-0.07	-0.067	2018	1.93	0.04	1.923
Core-2	1.95	-0.065	-0.066	-0.064	2015	1.97	-0.02	2.013
Core-3	1.94	-0.062	-0.063	-0.061	2012	1.94	0.00	2.013
Core-4	1.93	-0.059	-0.059	-0.058	2009	2.02	-0.08	1.873
Core-5	1.92	-0.055	-0.056	-0.055	2005	1.97	-0.05	1.953
Core-6	1.91	-0.052	-0.053	-0.051	2002	1.94	-0.03	1.923
Core-7	1.90	-0.049	-0.05	-0.048	1999	1.97	-0.06	2.053
Core-8	1.89	-0.046	-0.047	-0.045	1996	1.95	-0.06	1.943
Core-9	1.88	-0.043	-0.045	-0.041	1993	1.98	-0.09	1.953
Core-10	1.87	-0.04	-0.042	-0.038	1990	1.92	-0.05	1.943
Core-11	1.86	-0.037	-0.04	-0.034	1987	1.91	-0.05	1.943
Core-12	1.85	-0.034	-0.036	-0.031	1984	1.97	-0.12	2.053
Core-13	1.84	-0.031	-0.034	-0.028	1981	2.00	-0.16	1.873
Core-14	1.83	-0.028	-0.031	-0.025	1978	1.98	-0.15	1.953
Core-15	1.82	-0.025	-0.03	-0.021	1975	1.94	-0.12	1.943
Core-16	1.81	-0.022	-0.028	-0.017	1972	1.99	-0.18	2.043
Core-17	1.80	-0.018	-0.023	-0.014	1968	1.99	-0.18	2.043
Core-18	1.79	-0.014	-0.019	-0.01	1964	1.99	-0.20	2.093
Core-19	1.78	-0.01	-0.017	-0.004	1960	2.00	-0.21	2.093
Core-20	1.77	-0.006	-0.014	0.001	1956	1.96	-0.19	1.923
Core-21	1.76	-0.002	-0.012	0.008	1952	1.96	-0.19	1.923
Core-22	1.75	0.006	-0.003	0.015	1944	2.01	-0.25	2.093
Core-23	1.74	0.015	0.004	0.026	1935	1.97	-0.22	1.913
Core-24	1.73	0.023	0.009	0.039	1927	1.94	-0.20	1.923
Core-25	1.72	0.032	0.013	0.053	1918	1.90	-0.18	1.923
Core-26	1.71	0.04	0.017	0.067	1910	1.92	-0.21	2.013
Core-27	1.70	0.088	0.044	0.143	1862	1.92	-0.22	1.853
Core-28	1.69	0.137	0.06	0.241	1813	1.89	-0.19	1.943
Core-29	1.68	0.185	0.073	0.34	1765	1.89	-0.20	1.923
Core-30	1.67	0.233	0.086	0.441	1717	1.86	-0.18	1.883
Core-31	1.66	0.281	0.099	0.542	1669	1.88	-0.22	1.923

Core-32	1.65	0.366	0.22	0.571	1584	1.92	-0.27	2.013
Core-33	1.64	0.45	0.33	0.607	1500	1.79	-0.15	1.883
Core-34	1.63	0.534	0.431	0.644	1416	1.73	-0.10	1.883
Core-35	1.62	0.619	0.527	0.699	1331	1.76	-0.14	1.83
Core-36	1.61	0.703	0.598	0.791	1247	1.81	-0.20	1.83
Core-37	1.60	0.806	0.654	0.952	1144	1.83	-0.22	1.883
Core-38	1.59	0.909	0.692	1.156	1041	1.69	-0.10	1.791
Core-39	1.58	1.013	0.723	1.373	937	1.71	-0.13	1.717
Core-40	1.57	1.116	0.751	1.587	834	1.79	-0.21	1.883
Core-41	1.56	1.219	0.771	1.805	731	1.78	-0.22	1.83
Core-42	1.55	1.312	0.869	1.855	638	1.79	-0.24	1.83
Core-43	1.54	1.405	0.937	1.902	545	1.83	-0.28	1.83
Core-44	1.53	1.499	1.006	1.957	451	1.91	-0.38	1.943
Core-45	1.52	1.592	1.059	2.037	358	1.84	-0.31	1.883
Core-46	1.51	1.685	1.109	2.148	265	1.90	-0.39	1.943
Core-47	1.50	1.786	1.32	2.177	164	1.83	-0.32	1.883
Core-48	1.49	1.886	1.536	2.212	64	1.81	-0.31	1.883
Core-49	1.48	1.986	1.742	2.251	-36	1.81	-0.33	1.883
Core-50	1.47	2.086	1.923	2.29	-136	1.78	-0.31	1.83
Core-51	1.46	2.187	2.048	2.364	-237	1.90	-0.43	1.943
Core-52	1.45	2.325	2.212	2.469	-375	1.89	-0.44	1.923
Core-53	1.44	2.463	2.37	2.581	-513	1.89	-0.45	1.923
Core-54	1.43	2.602	2.528	2.697	-652	1.87	-0.44	1.853
Core-55	1.42	2.74	2.678	2.832	-790	1.81	-0.39	1.883
Core-56	1.41	2.879	2.816	2.986	-929	1.84	-0.43	1.83
Core-57	1.40	2.927	2.864	3.019	-977	1.74	-0.34	1.803
Core-58	1.39	2.975	2.901	3.056	-1025	1.81	-0.42	1.83
Core-59	1.38	3.023	2.934	3.111	-1073	1.82	-0.44	1.83
Core-60	1.37	3.071	2.968	3.176	-1121	1.94	-0.57	1.923
Core-61	1.36	3.12	2.996	3.248	-1170	1.95	-0.59	1.923
Core-62	1.35	3.156	3.046	3.267	-1206	1.93	-0.58	1.943
Core-63	1.34	3.192	3.082	3.297	-1242	1.97	-0.63	1.913
Core-64	1.33	3.229	3.11	3.331	-1279	1.97	-0.64	1.913
Core-65	1.32	3.265	3.129	3.374	-1315	1.95	-0.63	1.913

S2. Wavelet analysis results